ACS Partner Journal

Journal of the American Society for Mass Spectrometry

pubs.acs.org/jasms

Article

Photochemical and Collision-Induced Cross-Linking of Lys, Arg, and His to Nitrile Imines in Peptide Conjugate Ions in the Gas Phase

Jiahao Wan, Mikuláš Vlk, Marianna Nytka, Tuan Ngoc Kim Vu, Karel Lemr,* and František Tureček*

Cite This: *J. Am. Soc. Mass Spectrom.* 2025, 36, 209−220

Read Online

ACCESS | Metrics & More | Article Recommendations | Supporting Information

ABSTRACT: We report a study of internal covalent cross-linking with photolytically generated diarylnitrile imines of N-terminal arginine, lysine, and histidine residues in peptide conjugates. Conjugates in which a 4-(2-phenyltetrazol-5-yl)benzoyl group was attached to C-terminal lysine, that we call RAAA-*tet*-K, KAAA-*tet*-K, and HAAA-*tet*-K, were ionized by electrospray and subjected to UV photodissociation (UVPD) at 213 nm. UVPD triggered loss of N_2 and proceeded by covalent cross-linking to nitrile imine intermediates that involved the side chains of N-terminal arginine, lysine, and histidine, as well as the peptide amide groups. Cross-linking yields were determined from UVPD-MS^2 measurements as 67%, 66%, and 84% for RAAA-*tet*-K, KAAA-*tet*-K, and HAAA-*tet*-K ions, respectively. CID-MS^3 of the denitrogenated ion intermediates from RAAA-*tet*-K, KAAA-*tet*-K, and HAAA-*tet*-K indicated overall cross-linking yields of 80%, 89%, and 80%, respectively. The nature of the cross-linking reactions and cross-link structures were investigated for RAAA-*tet*-K by high-resolution cyclic ion mobility mass spectrometry that identified precursor ion conformers and multiple dissociation products. All sequences were subjected to conformational analysis by Born−Oppenheimer molecular dynamics, and energy analysis by density functional theory calculations with M06-2X/def2qzvpp that provided relative and dissociation energies for several cross-link structural types. The cross-linking reactions were substantially exothermic, driving the efficient conversion of nitrile-imine intermediates to cyclic products. The principal steps in covalent cross-linking involved proton transfer onto the nitrile imine group accompanied by nucleophilic attack by the peptide side-chain and amide groups. Blocking the proton transfer and nucleophile resulted in a loss of cross-linking abilities.

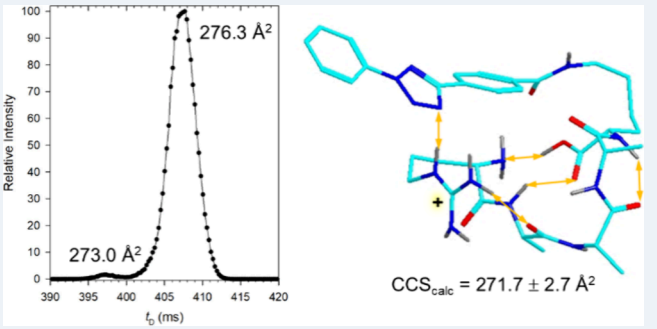

INTRODUCTION

Nitrile imines are reactive intermediates that have been used in organic chemistry for the synthesis of various nitrogen heterocycles.[1] Nitrile imines show particular reactivity to polar double bonds, such as those in methylene malonates and nitriles, but also have been found to react with nucleophilic groups.[2] In addition to their broad utility for organic synthesis, nitrile imines have been proposed as reagents in biomolecular cross-linking.[3] The nitrile-imine intermediate is generated by photodissociation of a suitable precursor, such as a diaryltetrazole group attached to the biomolecule, and allowed to react with a nucleophilic group (X_N) in the target compound to form a covalent bond (Scheme 1). The Scheme 1 reactions have been employed in a few studies of protein cross-linking where the diaryltetrazole was attached as an amide to the lysine ε-NH_2 group, and the reactive nucleophile was an aspartic acid side-chain carboxyl.[4,5]

Nitrile imines have been reported to be efficient cross-linkers in gas-phase peptide conjugates and noncovalent complexes.[6] In contrast to their condensed phase reactions, the nitrile-imine reactivity in the gas-phase cations is thought to be enhanced by intramolecular proton transfer forming transient nitrile-iminium ions of increased electrophilicity. This has been shown to activate nitrile imines to react with weak nucleophiles, such as peptide amide groups and nucleobases in complexes with oligonucleotides.[6] We have previously investigated nitrile-imine cross-linking to N-terminal amino acid residues in singly charged peptide ions containing Asp and Glu carboxyl and Asn and Gln carboxamide groups.[7] These have shown dual reactivity, whereby cross-linking was mediated to different degrees by the carboxyl or carboxamide, as well as by the peptide chain amide groups. Nitrile-imine cross-linking to C-terminal carboxyl groups has been reported for stereochemically distinct peptide scaffolds.[8]

Here, we explore the reactivity of N-terminal residues possessing basic and nucleophilic functionalities, such as a primary amine group in lysine, a guanidine group in arginine, and an imidazole ring in histidine. The peptide conjugates we

Received: October 31, 2024
Revised: November 29, 2024
Accepted: December 6, 2024
Published: December 18, 2024

Scheme 1. Cross-linking of Nitrile-Imine Intermediates with Target Nucleophiles

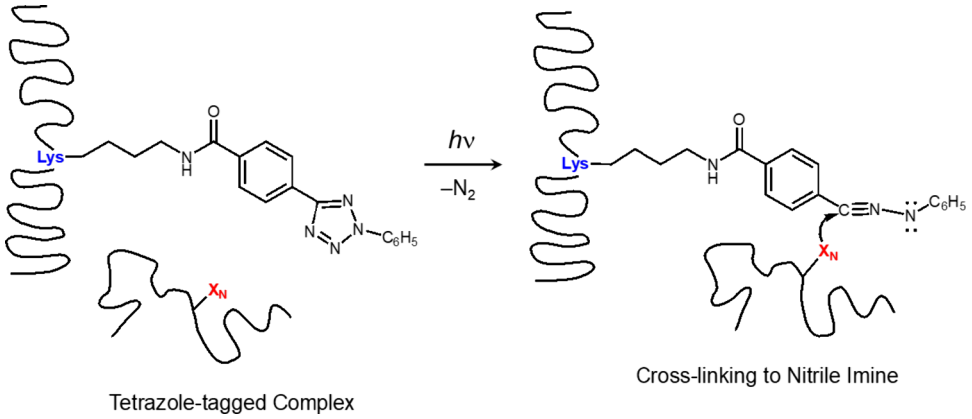

investigated carried the 2,5-diaryltetrazole group (*tet*) attached as an amide at the C-terminal lysine residue. These are denoted as KAAA-*tet*-K, RAAA-*tet*-K, and HAAA-*tet*-K. The basic amino acid residues in peptides are known to lower the peptide ion reactivity toward backbone cleavage by sequestering the charging proton and making it energetically less favorable for amide protonation.[9−11] From the cross-linking point of view, this could be a favorable feature because it may competitively enhance tetrazole ring cleavage upon nonspecific, collision-induced excitation. In this way, nitrile imines can be generated by both UV photodissociation (UVPD) and collision-induced dissociation (CID), which expands the options for further ion structure analysis by UVPD and CID tandem mass spectrometry, as well as by high-resolution ion mobility measurements. Conversely, the high basicity of Lys, Arg, and His functional groups may interfere with proton transfer to the nitrile imine to hamper cross-linking reactivity. We wish to show by experiment and theory that the arginine, lysine, and histidine basic/nucleophilic groups are reactive toward nitrile imines. To that end, we use a combination of tandem and cyclic ion mobility mass spectrometry and theoretical conformational and energy analysis to detect and identify the likely cross-link structures.

EXPERIMENTAL SECTION

Materials and Methods. Peptide conjugates with 4-(2-phenyl-2*H*-tetrazol-5-yl)benzoic acid (Sigma-Aldrich, St. Louis, MO), were synthesized by standard Fmoc coupling methods as reported previously.[6] The peptides were characterized by accurate m/z measurements and sequencing of electrosprayed ions in high-resolution mass spectrometry. The ε-*N*,*N*,*N*-trimethyl lysine derivative was prepared by exhaustive methylation of *N*-t-Boc-protected lysine that was built into the peptide sequence. For synthetic details, see the Supporting Information. Multistage UV photodissociation (UVPD) and CID-MS^n spectra were measured on an Orbitrap Ascend Tribrid instrument (ThermoFisher, San Jose, CA). For UVPD at 213 nm, we used multiple scans with a 20 ms stage time (33 laser pulses per scan) at 1.5 ± 0.2 μJ/pulse. Spectra were acquired by scanning the ion trap, or in the high-resolution mode in the Orbitrap at 125 000 resolving power. Accurate m/z and ion assignments are shown in Tables S1−S4 (Supporting Information). Ion mobility measurements were carried out on a SELECT SERIES Cyclic Ion Mobility Spectrometer (c-IMS) (Waters Corp., Wilmslow, U.K.)[12] with direct infusion into a normal flow electrospray ion source at a flow rate of 5 μL/min. Each sample and calibrant were measured six times in a positive mode. Typically, ion mobility separation over several cycles (n) was used at the total ion path of $n \times 98$ cm. Details of all measurement parameters and calibration for collision cross section (CCS) determination have been reported previously.[6]

Calculations. Born−Oppenheimer molecular dynamics (BOMD) calculations were carried out as described previously.[13] Briefly, multiple initial ion conformers were built in which the charging proton was placed on the basic residue (R, K, or H). BOMD trajectories were run for 20 ps at 510, 610, and 810 K with PM6-D3H4 that included empirical dispersion and hydrogen bonding interactions.[14] These calculations were run on the high-level Cuby4 platform[15] using MOPAC.[16] Inspection of the trajectories revealed that the systems were reaching a near-stationary state after ca. 16000 steps (16 ps), as determined by low root-mean-square deviations of atomic Cartesian coordinates, and so no longer trajectory runs were necessary because they generated only duplicate structures. The Berendsen thermostat[17] was used for energy stabilization. Two hundred snapshots were extracted from each trajectory at regular 100 fs intervals, and the geometries were gradient-optimized with PM6-D3H4. These were sorted out to weed out duplicates, and 20−30 lowest-energy structures were optimized with B3LYP[18] and M062X[19] with the 6-31+G(d,p) basis set including B3LYP/6-31+G(d,p) harmonic frequency analysis. The B3LYP calculations were augmented by including empirical dispersion corrections (GD3-BJ).[20,21] The M06-2*X*/6-31+G(d,p) optimized geometries were used to calculate single-point energies; these calculations used M06-2X and the def2qzvpp[22] basis set (up to 4635 basis functions). Basis set superposition error (BSSE) corrections were not applied when calculating the ion dissociation energies because the def2qzvpp basis set nearly reaches the complete basis set limit where BSSE becomes negligible.[23] Another set of M06-2*X*/6-31++G(d,p) single-point calculations were used to obtain charge densities according to Merz, Singh, and Kollman (MK).[24,25] All the standard DFT calculations were run using Gaussian 16 (Revision B.01) that was licensed from Gaussian, Inc. (Wallingford, CT). Collision cross sections in nitrogen (CCS_{calc}) were calculated by the modified ion trajectory method ($MobCal_{MPI}$)[26,27] using the MK charge densities. Ten trajectories were run amounting to 595840 points. Average CCS_{calc} values are reported with standard deviations. Standard

https://doi.org/10.1021/jasms.4c00438
J. Am. Soc. Mass Spectrom. 2025, 36, 209−220

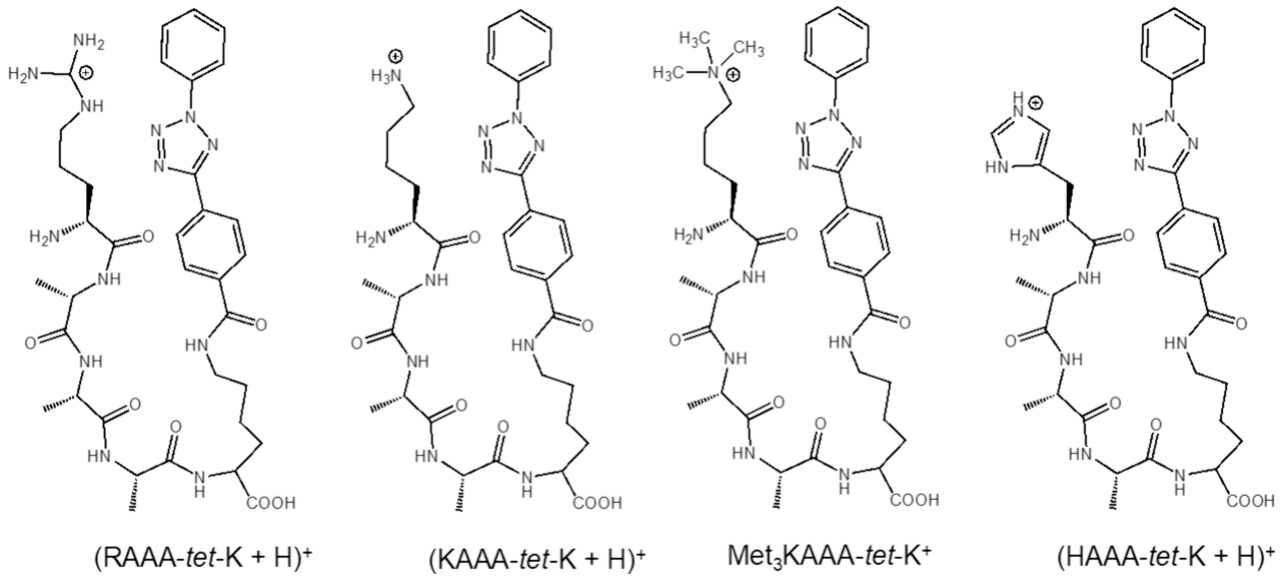

Figure 1. Peptide-tetrazole conjugate ions.

van der Waals parameters for different atom types were obtained from the MMFF94 data set.[28]

RESULTS AND DISCUSSION

Electrospray ionization of RAAA-*tet*-K, KAAA-*tet*-K, and HAAA-*tet*-K chiefly produced singly charged ions (Figure 1) that were selected by mass and investigated by tandem mass spectrometry. These sequences will be discussed separately, starting with RAAA-*tet*-K.

RAAA-*tet*-K. UVPD and CID-MS^2 of the (RAAA-*tet*-K + H)$^+$ ions (m/z 764) resulted in efficient loss of N_2 initially forming the m/z 736 nitrile-imine ion (Figure 2a, Figure S1a, Supporting Information). Both UVPD and CID triggered further dissociations of the (RAAA-*tet*-K − N_2 + H)$^+$ ions that produced two types of fragment ions. One type, which is present in particular upon UVPD, was by loss of C_6H_5N from the nitrile imine group (m/z 645). According to our previous data and interpretation,[6] this fraction was assigned to linear nitrile-imine intermediates. In addition, there was a $C_{14}H_9N_2O$ fragment ion that was characteristic of the free nitrile imine moiety. The main ion series commenced with the m/z 622 ion that was formed by loss of $C_5H_{10}N_2O$ from the denitrogenated ion. The other ions in this series were at m/z 551, 480, and 409 that sequentially differed by an [Ala] residue. UVPD-MS^2 further displayed a major $C_{15}H_{11}N_4O$ fragment ion in which the nitrile imine contained a covalently linked CH_2N_2 group originating from the Arg side chain. The nature of the (RAAA-*tet*-K − N_2 + H)$^+$ ions was further probed by UVPD-CID-MS^3 (Figure 2b) and CID-CID-MS^3 (Figure S1b, Supporting Information) that gave the same types of fragment ions. The chief fragment ions, besides the m/z 719 by loss of NH_3, were the m/z 622, 551, 480, and 409 C-terminal sequence ions in which a CH_2N_2 group from the Arg side chain was embedded in the nitrile imine group. We considered ions in this series, which are annotated as υ_1-υ_4 to distinguish them from standard [y_i + 2H]$^+$ ions,[29] as evidence for cross-linking by the Arg guanidine group. The CID-MS^3 spectra also displayed ions related to linear, non-cross-linked structures, such as the [y_2 + 2H]$^+$ (m/z 438) and [b_4 + H_2O]$^+$ (m/z 388) ions. All assignments were corroborated by accurate mass measurements (Table S1) and CID-MS^n of H/D exchanged ([D_{12}]-RAAA-*tet*-K + D)$^+$ and ([D_{12}]-RAAA-*tet*-K − N_2 + D)$^+$ ions (Figure S2a,b, Supporting Information). Dissociations of (RAAA-*tet*-K − N_2 + H)$^+$ ions were also studied under much harsher energy conditions of 213 nm CID-UVPD-MS^3

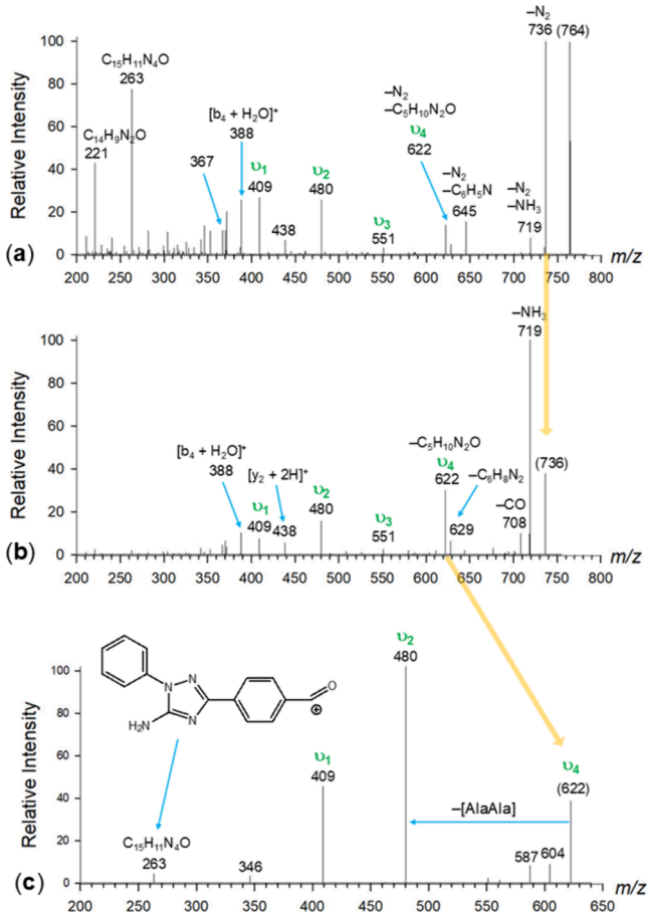

Figure 2. (a) UVPD-MS^2 of (RAAA-*tet*-K + H)$^+$ (m/z 764); (b) UVPD-CID-MS^3 of (RAAA-*tet*-K − N_2 + H)$^+$ (m/z 736); (c) CID-MS^4 of the υ_4 ions (m/z 622) from the Figure 2b spectrum.

https://doi.org/10.1021/jasms.4c00438
J. Am. Soc. Mass Spectrom. 2025, 36, 209−220

Scheme 2. Cross-Linking and Backbone Dissociations in $(RAAA\text{-}tet\text{-}K + H)^+$

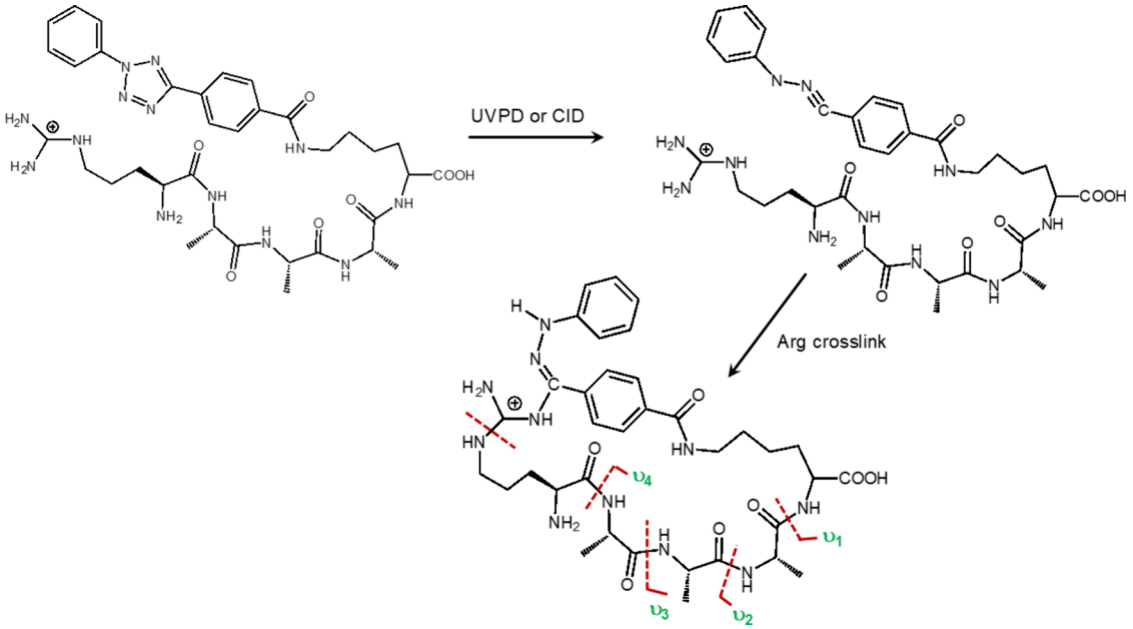

Scheme 3. Structures and Energies for the Formation of Nitrile Imines and $C_5H_{10}N_2O$ Loss from Arg-Cross-Linked Ions[a]

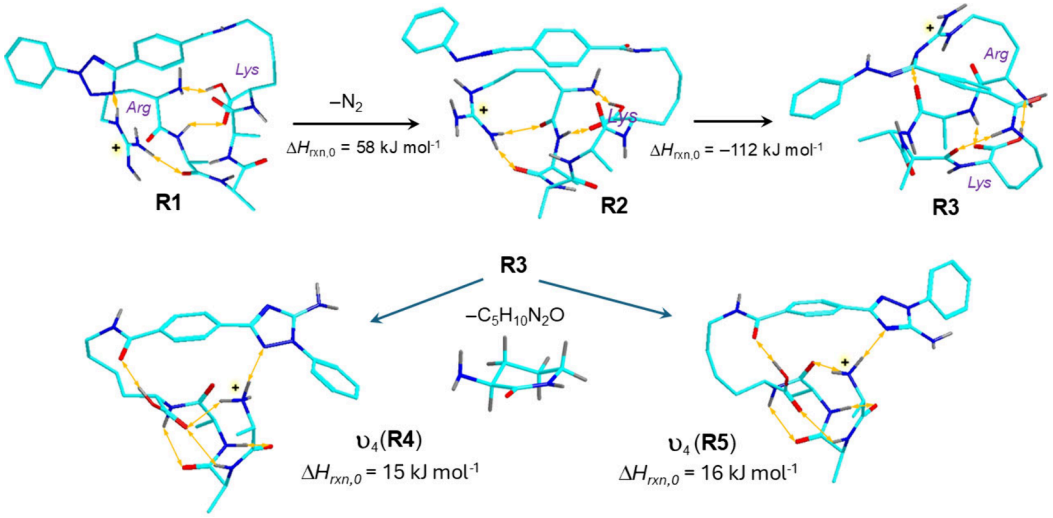

[a]Atom color coding is as follows: cyan = C, blue = N, red = O, gray = H. Only exchangeable N−H and O−H hydrogens are displayed to avoid clutter. Hydrogen bonds are annotated by ochre double-headed arrows. The relative Gibbs free energies are from M06-2X/def2qvzpp calculations and include B3LYP/6-31+G(d,p) zero-point energies.

(Figure S1c). In addition to the formation of the $\boldsymbol{v_1}$-$\boldsymbol{v_4}$ ions, UVPD resulted in deep dissociation forming the $C_{15}H_{11}N_4O$ ion (m/z 263) and a number of low-mass fragment ions. Overall, the information obtained from CID-UVPD was equivalent to that provided by UVPD-CID and CID-CID. The $\boldsymbol{v_4}$ sequence ion (m/z 622) that was indicative of arginine cross-linking was further studied by CID-MS^4. The spectrum (Figure 2c) showed dominant $\boldsymbol{v_2}$ ions by loss of [AlaAla]. We presumed that the facile loss of [AlaAla] was enabled by the formation of a cyclic 3,6-dimethyl-2,5-diketopiperazine neutral fragment that can arise from the combination of the Ala2-Ala3 or Ala3-Ala4 residues (Scheme 2).

To elucidate the structure and formation of the $\boldsymbol{v_4}$ sequence ions, we studied the dissociation energetics using DFT calculations following BOMD conformational analysis of the reactants and products. Loss of N_2 from the lowest-energy $(RAAA\text{-}tet\text{-}K + H)^+$ conformer (**R1**) was 58 kJ mol^{-1} endothermic, forming nitrile-imine intermediate **R2** which was the lowest-energy conformer among these ions. This very low reaction endothermicity did not include a barrier to the tetrazole ring opening which must be significantly higher to make the tetrazole ring stable at room temperature. Loss of N_2 has been known to compete with peptide bond cleavage in nonbasic peptides.[8] This indicated that the energy needed to open the tetrazole ring should be comparable to that for the peptide amide bond dissociation which has been reported to range within 160−263 kJ mol^{-1}.[30−33] While the activation energy for the ring opening in 2,5-diaryltetrazoles has not been measured, data for other tetrazoles have indicated activation energies of 193−194 kJ mol^{-1}.[34,35] Cross-linking by the Arg

https://doi.org/10.1021/jasms.4c00438
J. Am. Soc. Mass Spectrom. 2025, 36, 209−220

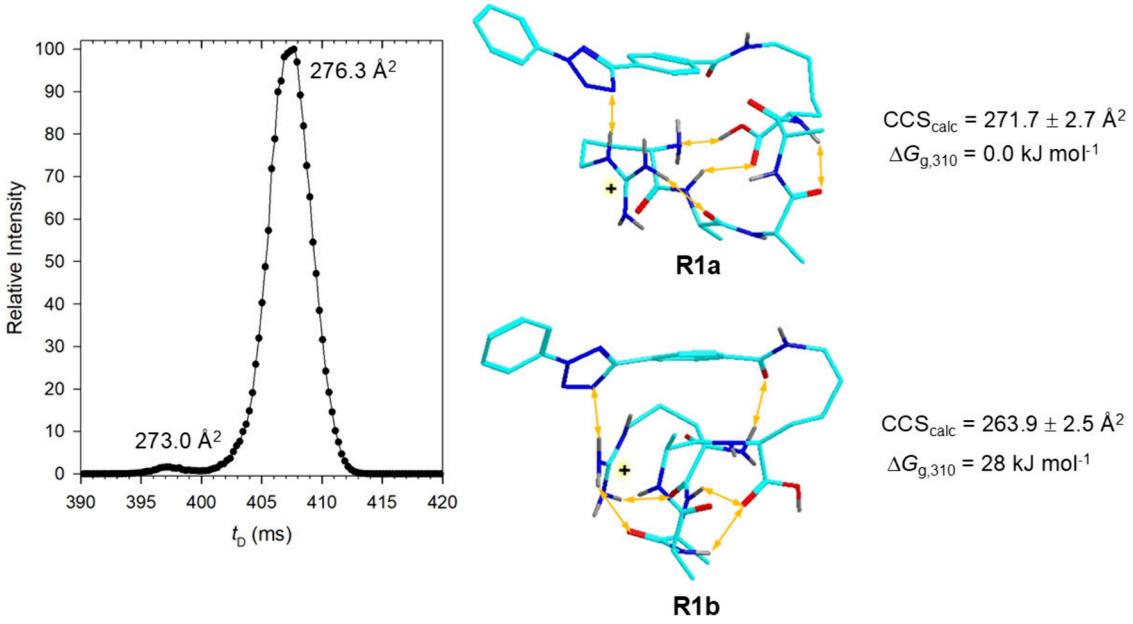

Figure 3. Left panel: Arrival time distribution of (RAAA-*tet*-K + H)$^+$ ions after 15 cycles (14.7 m path length). Right panel: M06-2X/6-31+G(d,p) optimized structures of lowest energy (RAAA-*tet*-K + H)$^+$ ions. Atom color coding is as in Scheme 3.

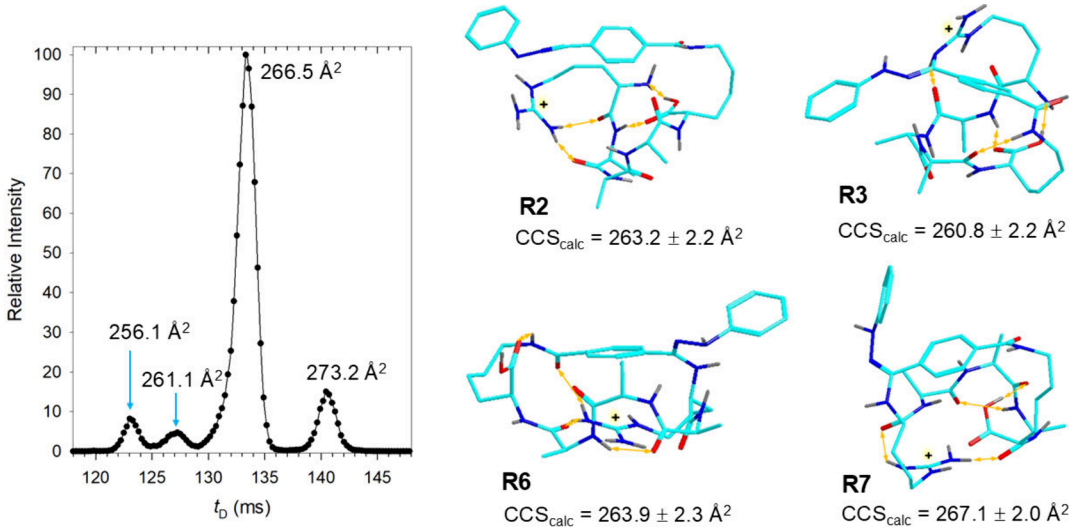

Figure 4. Left panel: Arrival time distribution of (RAAA-*tet*-K − N_2 + H)$^+$ ions after 5 cycles (490 cm path length). Right panel: M06-2X/6-31+G(d,p) optimized structures of representative lowest energy (RAAA-*tet*-K − N_2 + H)$^+$ ions. Atom color coding is as in Figure 3.

guanidine group in **R2** was substantially exothermic, $\Delta H_{rxn,0}$ = −112 kJ mol^{-1}, forming ion **R3** (Scheme 3).

It should be noted that proton transfer onto the nitrile-imine group in **R2** was a complex process reminiscent of proton migrations in other arginine-containing reactive peptide intermediates.[36] The BOMD trajectory of the nitrile-imine-protonated structure showed rapid proton migrations within 20 ps, forming NH_3^+...$^-$OCO zwitterions with a neutral guanidine group. The lowest energy structure (**R8**, Scheme S1, Supporting Information) indicated that protonated nitrile-imine was a reactive intermediate at ΔG_{310} = 140 kJ mol^{-1} relative to **R2** that collapsed exothermically to cross-link **R3**. The relative energies indicated that there was an energy barrier of at least 140 kJ mol^{-1} for the **R2** → **R3** reaction.

The further loss of the $C_5H_{10}N_2O$ molecule from **R3**, as indicated by CID-MS^3, had very low threshold energies of 15−16 kJ mol^{-1}, producing conformers **R4** and **R5**, respectively. This was established for a cyclic lactam structure for the Arg $C_5H_{10}N_2O$ fragment, as shown in Scheme 3. In addition, the H_2N−C═N group that was transferred to the nitrile imine in the course of cross-linking was found to spontaneously cyclize, forming a 1,2,4-triazole ring in the virtually isoenergetic conformers of the $\boldsymbol{v}_4$ ion (Scheme 3). The intermediate reaction steps leading to the $\boldsymbol{v}_4$ ion and $C_5H_{10}N_2O$ fragment formation, such as the Arg-Ala peptide bond and guanidine N−C bond cleavages, and accompanying proton migrations, likely had energy barriers exceeding the threshold energies that we did not address by calculations. Nevertheless, the very low threshold energies were consistent with the prominent $\boldsymbol{v}_4$ ion formation.

To further analyze the (RAAA-*tet*-K + H)$^+$ and (RAAA-*tet*-K − N_2 + H)$^+$ ions we used cyclic ion mobility to separate isomers and obtain collision cross sections (CCS$_{exp}$). Ion mobility showed a major isomer (94%) with CCS$_{exp}$ = 276.3 Å^2

https://doi.org/10.1021/jasms.4c00438
J. Am. Soc. Mass Spectrom. 2025, 36, 209−220

that was accompanied by a more compact minor isomer with CCS_{exp} = 273.0 Å^2 (Figure 3, left panel). According to the calculations, the lowest energy structure **R1a** had a CCS_{calc} = 271.7 ± 2.7 Å^2. A more compact but substantially less stable isomer (**R1b**) had CCS_{calc} = 263.9 ± 2.5 Å^2. The agreement between the experimental and calculated CCS for **R1a** (Δ_{rel} = 1.7%), albeit still remarkably good, showed a slightly larger difference than those reported for other peptide ions.[6−8] The minor component remained unidentified and may correspond to a higher-energy conformer. The lowest-energy structure **R1a** showed a tightly folded peptide chain that was supported by multiple hydrogen bonds. Those included guanidinium group H-bonding to the Ala2 amide and the tetrazole ring (Figure 3). The conformer near-homogeneity of the (RAAA-*tet*-K + H)$^+$ ions, as displayed by the arrival time distribution, was consistent with the relatively large gap in the Gibbs free energies (28 kJ mol^{-1}) separating **R1a** from **R1b** and other higher energy isomers.

The (RAAA-*tet*-K − N_2 + H)$^+$ ions used for ion mobility measurements were generated by CID-MS^2. Owing to the similarity of the CID-MS^3 spectra of (RAAA-*tet*-K − N_2 + H)$^+$ made by CID and UVPD (Figure 2b and Figure S1b, respectively), we presume that the formation and composition of isomers were similar in both activation modes. The arrival time distribution of (RAAA-*tet*-K − N_2 + H)$^+$ ions, obtained after 5 cycles (490 cm path length), showed multiple components (Figure 4, left panel). The dominant component had CCS_{exp} = 266.5 Å^2 that was flanked by more compact minor components of CCS_{exp} = 256.1 Å^2 and 261.1 Å^2 and a more expanded component of CCS_{exp} = 273.2 Å^2. To assign plausible structures for the (RAAA-*tet*-K − N_2 + H)$^+$ ions, we considered linear nitrile-imine conformers, as well as cross-links by the Arg side-chain guanidine and N-terminal amine groups. This selection was guided by the dissociations observed in the UVPD-MS^2 and CID-MS^3 spectra, as discussed above. When considering low-energy conformers in each group, the CCS_{calc} of 17 isomers ranged from 255.9 Å^2 through 267.1 Å^2 which covered the range of CCS_{exp}. Individual peak assignment was less specific because of the multitude of structures and the uncertainty in matching CCS_{calc} with CCS_{exp} that can be estimated as within ca. 2% or 5 Å^2 (see above). The lowest energy structures in each group are depicted in Figure 4. The Arg-cross-linked ion **R3** had CCS_{calc} = 260.8 Å^2 which was on the low side of the major peak in the mobilogram. Ion **R3** had a compact structure that was secured by the Arg cross-link and included proton transfer onto the nitrile imine in addition to cyclization. The nitrile-imine isomer **R2** of CCS_{calc} = 263.2 Å^2 made it closer to the major peak in the mobilogram. Two other isomers, **R6** and **R7**, were cross-linked by the N-terminal amine group. Their CCS_{calc} = 263.9 and 267.1 Å^2 for **R6** and **R7**, respectively, also fell within the experimental range and were close to the CCS_{exp} of the main peak. We note that ion **R6** was the global energy minimum of the entire set at ΔG_{310} = −30 kJ mol^{-1} relative to **R3**. Nitrile imine **R2** was at ΔG_{310} = 106 kJ mol^{-1} relative to **R3**, indicating the high exothermicity of cross-link formation. Two points are noteworthy in this respect. First, the relative energies of cross-links of a different type, such as **R3** and **R6**, were not indicative of their competitive formation from nitrile imines. This is because the cross-linking reactions were determined by the pertinent activation energies and, once formed, the isomers were unlikely to interconvert. Second, the match between the hypothetical CCS_{calc} and measured CCS_{exp} did not guarantee structure assignment. This was particularly evident from the CID-MS^3 spectra that did not indicate the presence of *N*-terminally cross-linked structures, for which a loss of [Ala] would be expected upon CID. Instead, the Figure S1b spectrum showed guanidine cross-linking to the nitrile-imine group, as indicated by the prominent υ_1-υ_3 fragment ion series.

KAAA-*tet*-K. Both UVPD and CID of (KAAA-*tet*-K + H)$^+$ (*m*/*z* 736) resulted in an efficient loss of N_2 (Figure 5a, Figure S3, Supporting Information, respectively). Higher excitation upon UVPD then led to consecutive dissociations of the denitrogenated *m*/*z* 708 ions; only a few of these dissociations were indicative of linear nitrile-imine structures, e.g., the *m*/*z* 617 ion by loss of C_6H_5N, and *m*/*z* 438 that according to its elemental composition was a denitrogenated [y_2 + 2H]$^+$ fragment ion. The chief dissociation channel was loss of $C_6H_8N_2$ that, according to deuterium labeling in ([D_{10}]-KAAA-*tet*-K + D)$^+$ (*m*/*z* 747, Figure S4, Supporting Information), contained three exchangeable protons and was identified as phenylhydrazine. This primary dissociation was followed by internal backbone cleavages expelling neutral [Ala] fragments and forming the *m*/*z* 529 and 458 ions (Figure 5a). Loss of phenyl hydrazine was also the predominant channel in CID-MS^3 of the *m*/*z* 708 ions forming the *m*/*z* 600 ion (Figure 5b). This dissociation required transfer of three hydrogen atoms onto the nitrile imine group and must have been associated with cross-linking to the remaining nitrile

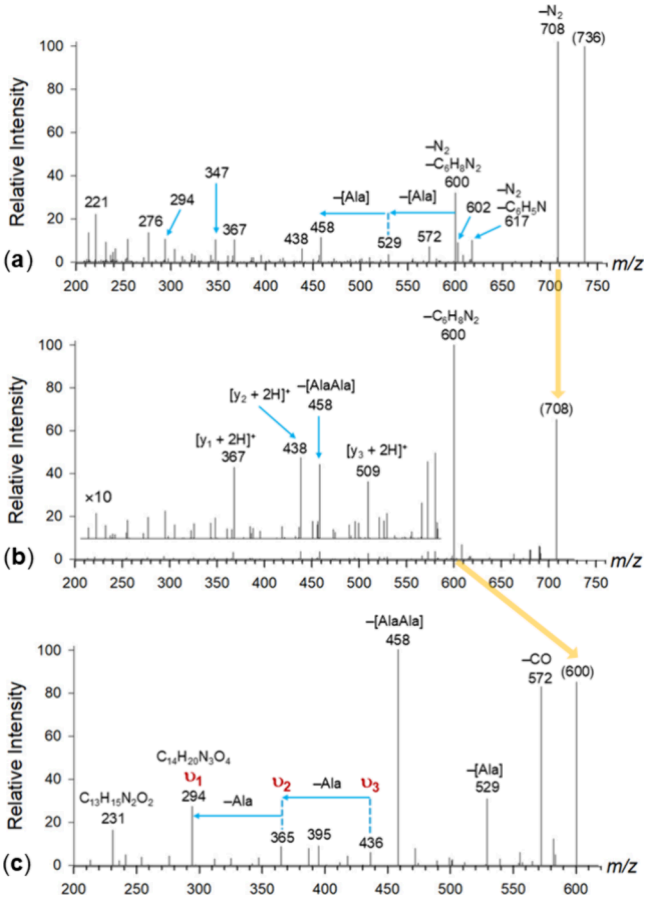

Figure 5. (a) UVPD-MS^2 of (KAAA-*tet*-K + H)$^+$ (*m*/*z* 736); (b) UVPD-CID-MS^3 of (KAAA-*tet*-K − N_2 + H)$^+$ (*m*/*z* 708); (c) CID-MS^4 of the *m*/*z* 600 ion from the Figure 5b spectrum.

https://doi.org/10.1021/jasms.4c00438
J. Am. Soc. Mass Spectrom. 2025, 36, 209−220

Scheme 4. Cross-Linking and Backbone Dissociations in $(KAAA\text{-}tet\text{-}K - N_2 + H)^+$

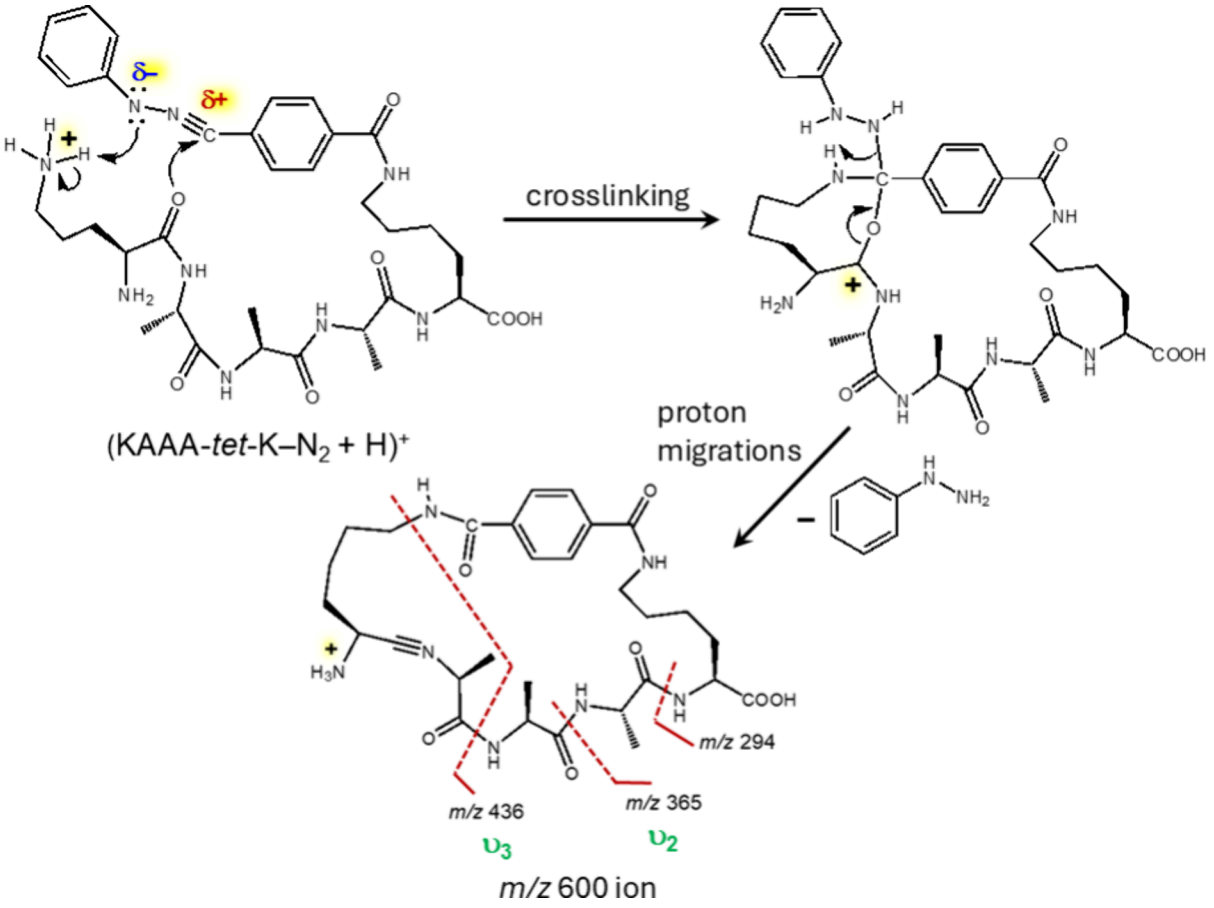

Scheme 5. Structures and M06-2X/def2qzvpp Relative Energies of $(KAAAK\text{-}tet\text{-}K + H)^+$ Ions

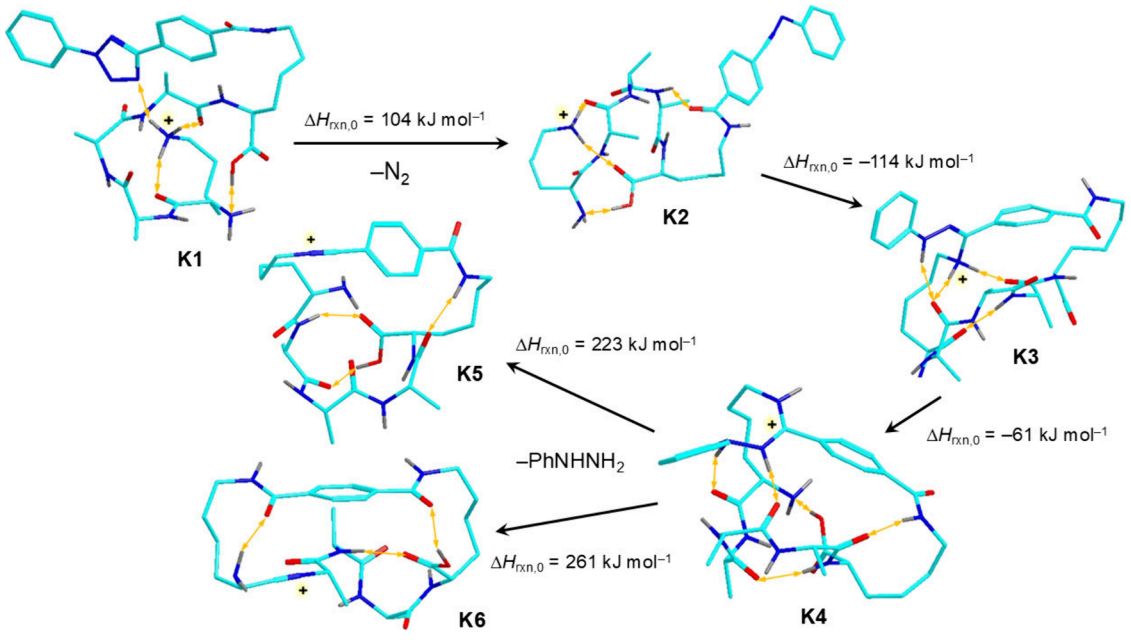

carbon atom in order to avoid a high-energy methine structure in the fragment ion. This was consistent with the internal backbone cleavages and loss of [Ala]. These were particularly evident in the UVPD-MS^3 spectrum of the m/z 708 ion (Figure S5, Supporting Information) that also displayed fragment ions resulting from deep secondary dissociations that were identified by their elemental composition (Table S2, Supporting Information). The nature of the cross-links was further elucidated by CID-MS^4 of the m/z 600 ion (Figure 5c). This showed losses of [Ala] and [AlaAla], m/z 529 and 458,

https://doi.org/10.1021/jasms.4c00438
J. Am. Soc. Mass Spectrom. 2025, 36, 209−220

respectively, indicating cross-linked structures. In addition, we identified a series of fragment ions separated by [Ala] at m/z 294, 365, and 436 that provided a clue to the cross-link bond connectivity. The m/z 294 ion, $C_{14}H_{20}N_3O_4$, was composed of the lysine residue that was attached to the benzoyl moiety containing a $CONH_2$ group that was not originally present in the nitrile imine. This group resulted from a combined or consecutive transfer of O and NH_2 unto the nitrile-imine carbon atom in the course of cross-link formation.

A possible reaction sequence for this transformation is sketched in Scheme 4, showing proton transfer to the nitrile-imine nitrogen, accompanied by the formation of the ε-N−C and O−C bonds to the nitrile-imine carbon atom. This produced an intermediate with a weak N−C bond that was prone to phenyl hydrazine elimination which was accompanied by another proton transfer. The m/z 600 ion, bottom structure in Scheme 4, can break any of the backbone amide bonds and eliminate CO, [Ala], or [AlaAla], which were the main observed dissociations. In addition, cleavage of the lysine C−ε-N bond, possibly promoted by proton transfer and assisted by N-terminal NH_2 participation, can open the macrocyclic ring and enable the formation of modified y-type ions that we denote as $\boldsymbol{\upsilon_1}$-$\boldsymbol{\upsilon_3}$ at m/z 294, 365, and 436, respectively, to distinguish them from standard $[y_i + 2H]^+$ ions. Notably, the absence of the lysine carbonyl prevents the formation of the $\boldsymbol{\upsilon_4}$ ion that was absent in the Figure 5c spectrum. It should be noted that the spectra alone did not allow us to distinguish between structures cross-linked by the side chain and N-terminal amine groups, and additional calculations and experiments were needed to resolve this issue.

We mapped the relevant parts of the KAAAK-*tet*-K ion potential energy surface to determine the dissociation and isomerization energies (Scheme 5). Starting from the lowest-energy $(KAAA\text{-}tet\text{-}K + H)^+$ conformer (**K1**), loss of N_2 was calculated to require 104 kJ mol^{-1} to form the lowest-energy nitrile imine **K2**. As discussed above, the overall dissociation endothermicity did not include the activation energy for the tetrazole ring opening. Ring closure in **K2** involving the Lys-ε-amine group was 114 kJ mol^{-1} exothermic, forming cross-link **K3** that could further isomerize by exothermic proton migration to the most stable isomer **K4**. We found two pathways for further dissociation of **K4** by loss of phenylhydrazine. In the first one, proton migration would weaken the $PhNHNH_2$−C bond, resulting in its dissociation forming ion **K5** that was 223 kJ mol^{-1} endothermic relative to **K4**. Ion **K5** was presumed to dissociate by [Ala] and [AlaAla] internal cleavages upon CID (Figure 5c). The other pathway included migration of an amide proton to trigger $PhNHNH_2$ loss with participation by the Lys amide, forming isomer **K6**. This reaction was 261 kJ mol^{-1} endothermic. Ion **K6** was a natural precursor for the formation of the $\boldsymbol{\upsilon_1}$-$\boldsymbol{\upsilon_3}$ fragment ions upon further CID (Figure 5c).

The role of the lysine ε-NH_2 group and proton transfer was investigated by using a derivative that was trimethylated at the side chain nitrogen, $(\varepsilon\text{-}(CH_3)_3KAAA\text{-}tet\text{-}K)^+$ which was a quaternary ammonium ion, m/z 778. The UVPD and CID-MS^2 spectra showed facile loss of N_2 (m/z 750, Figure S6a,b, Supporting Information). However, all backbone dissociations upon MS^2 as well as CID-MS^3 gave standard $[y_n + 2H]^+$ fragment ions, m/z 367, 438, 509, and 580 (Figure S6c, Supporting Information). No fragment ions indicating cross-links were observed. A side-reaction observed for $(\varepsilon\text{-}(CH_3)_3KAAA\text{-}tet\text{-}K - N_2)^+$ was the loss of $(CH_3)_3N$, giving rise to the m/z 691 fragment ion. CID-MS^4 of this ion showed a complete series of $[y_n + 2H]^+$ fragment ions in addition to complementary $\boldsymbol{b_n}$ − $(CH_3)_3N$ ions (Figure S6d, Supporting Information). Another side reaction revealed by the spectra was a methyl transfer from the Lys $(CH_3)_3N$ group followed by reverse proton migration forming the charged $(CH_3)_2NH$ group. This resulted in a minor dissociation by loss of $C_8H_{18}N_2$ (m/z 608, Figure S6) and subsequent backbone cleavages by loss of internal [Ala]. These minor reactions contributed to the small fractions of cross-links from $(\varepsilon\text{-}(CH_3)_3KAAA\text{-}tet\text{-}K)^+$ as listed in Table 1. We note that intramolecular methyl transfer from the trimethylammonium group onto nucleobases has been reported previously.[37] Since lysine trimethylation accomplished the functions of blocking both the nucleophilic attack and proton transfer to the nitrile imine, these effects were not clearly distinguished. However, as reported previously, N-terminal amino acid residues lacking nucleophilic groups did undergo cross-linking to nitrile imines by using the peptide amide group. Since this reaction was absent with $(\varepsilon\text{-}(CH_3)_3KAAA\text{-}tet\text{-}K)^+$, we tend to conclude that it was the lack of a transferrable proton that blocked cross-linking in these gas-phase ions. This conclusion was consistent with previous results with sodiated ions that also did not undergo cross-linking to nitrile imines.[6]

Table 1. Yields of Cross-Linked Products

sequence	UVPD conversion[b]	cross-link yield[a] UVPD-MS^2	cross-link yield[a] UVPD-CID-MS^3
RAAA-*tet*-K	36	67	80
KAAA-*tet*-K	40	66	89
ε-$(CH_3)_3$KAAA-*tet*-K	31	0.8[c]	2.1[c]
HAAA-*tet*-K	25	84	80

[a]Calculated as the percentage of the sum of intensities of identified cross-linked fragment ions relative to the sum of intensities of all sequence fragment ions. [b]Sum of identified UVPD product ion intensities relative to the precursor ion intensity. [c]From rearranged $(\varepsilon\text{-}(CH_3)_2KAAA\text{-}tet\text{-}K + CH_3)^+$ ions.

HAAA-*tet*-K. UVPD and CID-MS^2 of $(HAAA\text{-}tet\text{-}K + H)^+$ (m/z 745) revealed a prominent loss of phenylhydrazine (m/z 609) after loss of N_2 (m/z 717) (Figure 6a, Figure S7, Supporting Information). In addition, UVPD resulted in deep dissociations within both the peptide chain and nitrile imine moiety, producing among others the $C_{14}H_9N_2O$ (m/z 221) and $C_{12}H_{16}N_6O_2$ (m/z 262) fragment ions (Table S4, Supporting Information). In addition to the loss of $C_6H_8N_2$, the spectra also showed loss of $C_5H_7N_3$ from the His residue giving rise to the m/z 608 ion. This was a characteristic dissociation of N-terminal amino acid residues in ions that were cross-linked to the nitrile imine by the peptide amide bond and rearranged to hydrazone structures.[6] Cross-linked structures were indicated by both UVPD and CID that displayed consecutive dissociation of the m/z 608 ions by expulsion of an internal [Ala] residue (m/z 537). The hydrazone cross-link can account for loss of both $C_5H_7N_3$ containing the His side chain, and phenylhydrazine as $C_6H_8N_2$ (Scheme 6). Both dissociations must be accompanied by proton migrations either from or to the neutral fragment. The ion assignment was corroborated by CID-MS^3 of the $([D_9]HAAAK - N_2 + D)^+$ ion (m/z 727) that showed the

https://doi.org/10.1021/jasms.4c00438
J. Am. Soc. Mass Spectrom. 2025, 36, 209−220

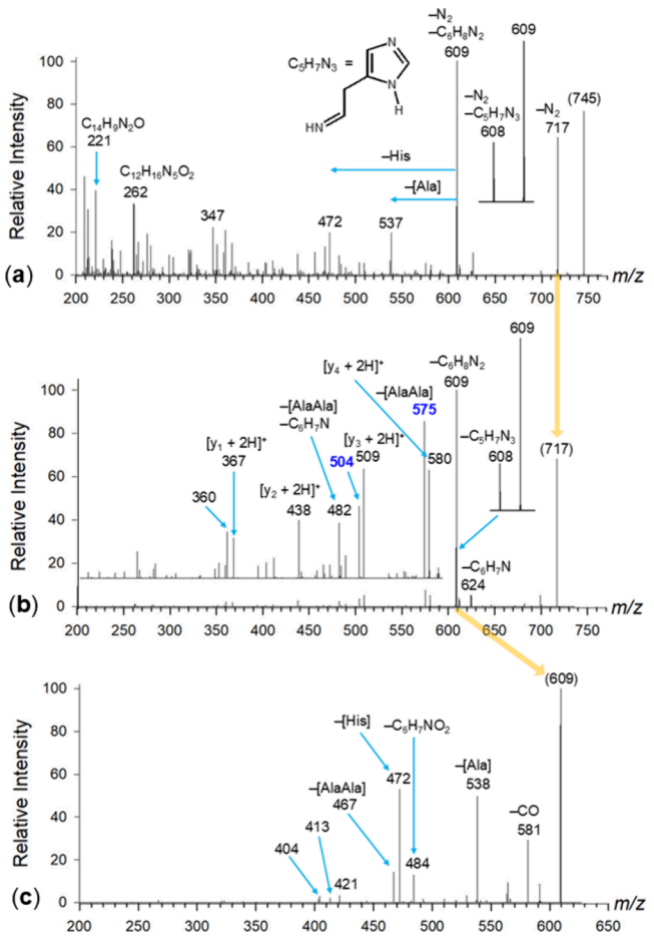

Figure 6. (a) UVPD-MS^2 of $(HAAA\text{-}tet\text{-}K + H)^+$ (m/z 745); (b) CID-MS^3 of $(HAAA\text{-}tet\text{-}K - N_2 + H)^+$ (m/z 717); (c) CID-MS^4 of $(HAAA\text{-}tet\text{-}K - N_2 - C_6H_8N_2 + H)^+$ (m/z 609).

fragment ions by loss of $C_6H_5D_3N_2$ and $C_5H_5D_2N_3$ as a partially resolved doublet at m/z 616.3177 and m/z 616.3290, respectively, in the high-resolution mass spectrum (Figure S8a, Supporting Information). This represented transfer of three exchangeable deuterium atoms onto the phenylhydrazine molecule in $C_6H_5D_3N_2$ and transfer of one exchangeable deuterium atom from the His amine group in $C_5H_5D_2N_3$ to the fragment ion. Loss of phenylhydrazine was also prominent in CID-MS^3 of the $(HAAAK - N_2 + H)^+$ ion (m/z 717) producing the m/z 609 fragment ion (Figure 6b). There was only weak further fragmentation that revealed the presence of cross-linked and linear nitrile-imine structures. Cross-links were represented by loss of [AlaAla] and [AlaAlaAla] internal residues (m/z 575 and 504, respectively). Linear structures were indicated by the $[y_i + 2H]^+$ ions at m/z 580, 509, 438, and 367 (Figure 6b). Further analysis of the m/z 609 ion by CID-MS^4 revealed loss of internal [Ala] and [AlaAla] fragments, but not [AlaAlaAla]. This was consistent with the suggested structure of the cross-linked ion where the Ala2 residue was bonded to the ring bridgehead. The side-chain dissociations starting from amide and His cross-linked structures are sketched in Scheme 6 and further investigated computationally.

We used BOMD and DFT calculations to assess the thermochemistry of cross-linking in $(HAAA\text{-}tet\text{-}K - N_2 + H)^+$ ions. The lowest energy $(HAAA\text{-}tet\text{-}K + H)^+$ precursor ion (**H1**) was protonated at the N-terminus. Structures that were started with a protonated His imidazole collapsed by proton transfer to N-terminally protonated ones upon BOMD. Loss of N_2 ($\Delta H_{rxn,0}$ = 120 kJ mol^{-1}) proceeded via nitrile imine **H2**, which was the lowest-energy conformer, showing a strong hydrogen bond between the charged N-terminal NH_3 group and one of the nitrile imine nitrogen atoms (Scheme 7). Cross-linking in **H2** by the imidazole ring could produce ion **H3**, which was the lowest-energy conformer of this type. As opposed to **H1**, charging in **H3** was favored at the cross-linked His imidazole ring whereas the ammonium proton was transferred to the hydrazidine moiety where it formed a strong hydrogen bond to the neutral *N*-terminal amine (Scheme 7). The formation of **H3** from **H2** was highly exothermic, $\Delta H_{rxn,0}$ = −109 kJ mol^{-1}, making the overall N_2 loss and cross-linking only 11 kJ mol^{-1} endothermic, and leaving this dissociation well within the range of excitation energies in **H1** after photon absorption or collisional activation. The alternative cross-linking that was associated with amide oxygen transfer onto the nitrile imine could produce ion **H4**. Although of somewhat higher energy than **H3**, the formation of **H4** from **H1** required 63 kJ mol^{-1} that was thermochemically facile considering the **H1** excitation energies.

Structure **H3** was a natural intermediate for the elimination of phenylhydrazine forming the m/z 609 ion **H5** (Scheme 7), which was the dominant dissociation of both $(HAAA\text{-}tet\text{-}K + H)^+$ and $(HAAA\text{-}tet\text{-}K - N_2 + H)^+$ (Figure 6a,b). The calculated enthalpy for the **H3** reaction dissociating to **H5** and phenylhydrazine, $\Delta H_{rxn,0}$ = 94 kJ mol^{-1}, was significantly lower

Scheme 6. Diagnostic Side-Chain Dissociations in Cross-Linked $(HAAA\text{-}tet\text{-}K - N_2 + H)^+$ Ions

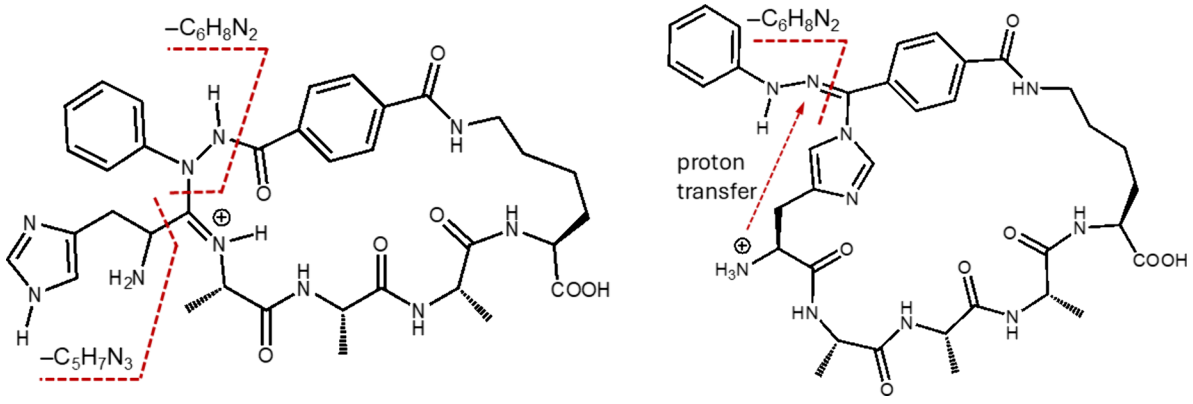

https://doi.org/10.1021/jasms.4c00438
J. Am. Soc. Mass Spectrom. 2025, 36, 209−220

Scheme 7. Structures and Dissociation Energies of HAAA-*tet*-K Ions

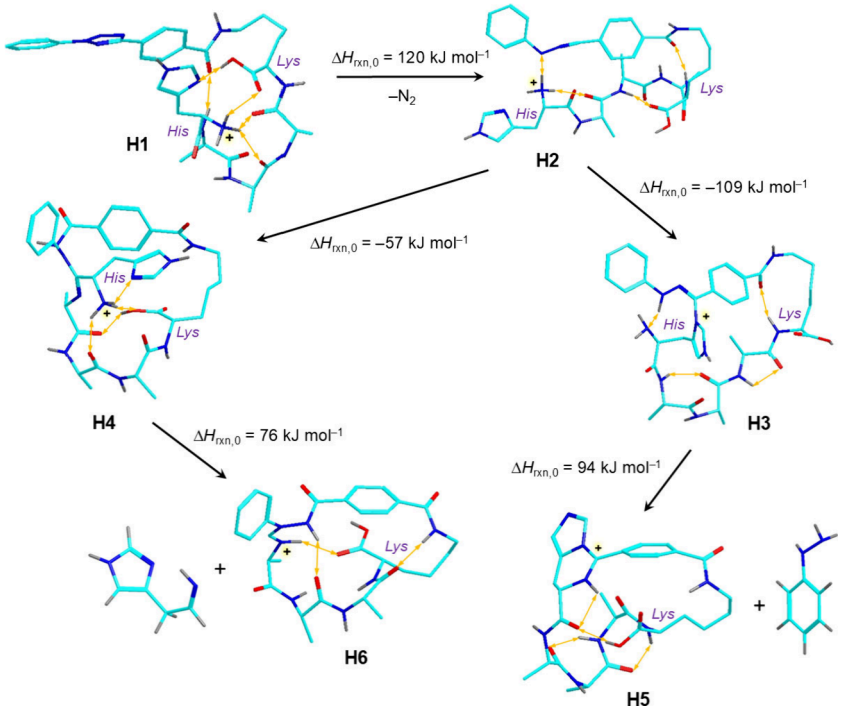

than typical energies for peptide ion backbone dissociations, as was the overall enthalpy needed for the **H1** → **H5** conversion with the consecutive loss of N_2 and phenylhydrazine, $\Delta H_{rxn,0}$ = 105 kJ mol^{-1}. This was consistent with the facile loss of phenylhydrazine that outcompeted all other dissociations, such as peptide backbone cleavages that typically require threshold energies in the 162−263 kJ mol^{-1} range.[30−33] Structure **H4** was a plausible precursor for the side-chain loss of imidazolylacetaldimine ($C_5H_7N_3$), giving rise to the *m*/*z* 608 fragment ion (Figure 6a,b). This dissociation, **H4** → **H6** + $C_5H_7N_3$, required a threshold energy of $\Delta H_{rxn,0}$ = 76 kJ mol^{-1} (Scheme 7) which was well within the range of the precursor ion excitation energies. The combined threshold energies for the formation from **H1** of **H5** and **H6**, $\Delta H_{rxn,0}$ = 105 and 139 kJ mol^{-1}, respectively, were in a qualitative agreement with the formation of the corresponding *m*/*z* 609 and *m*/*z* 608 fragment ions where the lower-energy former dissociation prevailed.

The data showed that all three basic residues, Arg, Lys, and His, engaged in cross-linking interactions with the nitrile-imine group. The types of chemical reactions were different for the arginine, lysine, and histidine residues, leading to products that showed different reactivity upon further collisional excitation, as discussed above. The most salient difference was found for the dissociation type that was elimination of phenylhydrazine for the lysine and histidine cross-links whereas the arginine cross-links broke up the guanidine group. Since the phenylhydrazine loss involved multiple proton transfers, its lower representation with arginine cross-links may be due to the substantially higher guanidine group basicity compared to the lysine NH_2 and histidine imidazole ring.

To assess the proclivity of the basic residues for the cross-linking reactions, we calculated the cross-link yields that were defined as percent of the sum of the intensities of ions identified as originating from cross-links relative to the sum of the intensities of all sequence ions. The yields are reported in Table 1. The data showed that the arginine, lysine, and histidine residues did not substantially differ in their cross-link yields. However, the distribution of cross-link-indicating fragment ions was very different for (RAAA-*tet*-K + H)$^+$ than for (KAAA-*tet*-K + H)$^+$ and (HAAA-*tet*-K + H)$^+$ (Figure S9, Supporting Information). This showed that the major fraction of cross-links in (RAAA-*tet*-K + H)$^+$ was due to the HN═C−NH_2 group transfer from arginine. A large difference was observed for *ε*-[$(CH_3)_3$KAAA-*tet*-K]$^+$ where cross-linking was severely hampered by the lack of a mobile proton, and only minor fractions of cross-linked ions were observed as a result of methyl transfer that mobilized a proton in the rearranged ion.

The similar overall cross-linking yields pointed to the high reactivity of the nitrile imine group. Judged by the optimized ion structures, the interacting groups can be remote in the lowest-energy nitrile imine conformers. However, owing to the high internal energy acquired by photodissociation or CID, the nitrile imine intermediates can undergo fast conformational changes, and those that bring the proton-donating and nucleophilic groups close to the nitrile imine are bound to result in exothermic cross-linking. This was evident from the analysis of BOMD trajectories for the nitrile imines that showed progressions of multiple conformations within 20 ps.

CONCLUSIONS

Basic amino acid residues with nucleophilic side-chain groups, as in Arg, Lys, and His, were found to react with nitrile imines in peptide conjugates, forming internally cross-linked products. This finding expands the scope of nitrile-imine based cross-linking to a variety of peptides ranging from those with nonbasic (Gly, Ala, Phe), through acidic (Asp, Glu), to weakly nucleophilic (Asn, Gln) and basic (Arg, Lys, His) amino acid residues. Experiments in which the proton donor and/or nucleophiles were blocked showed substantially diminished reactivity toward nitrile imines. Cross-linking in peptide

https://doi.org/10.1021/jasms.4c00438
J. Am. Soc. Mass Spectrom. 2025, 36, 209−220

conjugates is readily recognized by the formation of internal fragments upon ion activation.

■ ASSOCIATED CONTENT

Supporting Information

The Supporting Information is available free of charge at https://pubs.acs.org/doi/10.1021/jasms.4c00438.

Synthetic procedures, high-resolution data, and auxiliary tandem mass spectra (PDF)

■ AUTHOR INFORMATION

Corresponding Authors

Karel Lemr − *Department of Analytical Chemistry, Faculty of Science, Palacký University, Olomouc 77900, Czech Republic; Institute of Microbiology of the Czech Academy of Sciences, Prague 14220, Czech Republic;* orcid.org/0000-0003-3158-0637; Email: karel.lemr@upol.cz

František Tureček − *Department of Chemistry, Bagley Hall, University of Washington, Seattle, Washington 98195-1700, United States;* orcid.org/0000-0001-7321-7858; Email: turecek@uw.edu

Authors

Jiahao Wan − *Department of Chemistry, Bagley Hall, University of Washington, Seattle, Washington 98195-1700, United States*

Mikuláš Vlk − *Department of Chemistry, Bagley Hall, University of Washington, Seattle, Washington 98195-1700, United States; Institute of Organic Chemistry and Biochemistry, Czech Academy of Sciences, Prague 16610, Czech Republic; Department of Analytical Chemistry, Faculty of Science, Charles University, Prague 12800, Czech Republic*

Marianna Nytka − *Department of Analytical Chemistry, Faculty of Science, Palacký University, Olomouc 77900, Czech Republic;* orcid.org/0000-0002-9242-8295

Tuan Ngoc Kim Vu − *Department of Chemistry, Bagley Hall, University of Washington, Seattle, Washington 98195-1700, United States*

Complete contact information is available at: https://pubs.acs.org/10.1021/jasms.4c00438

Notes

The authors declare no competing financial interest.

■ ACKNOWLEDGMENTS

Research at the University of Washington was supported by the Chemistry Division of the U.S. National Science Foundation, Grant CHE-2347921. F.T. acknowledges support by the Klaus and Mary Ann Saegebarth Endowment. M.V. acknowledges support from the Charles University research project SVV260690. Research at Palacký University was supported by projects IGA PrF 2023 027 and IGA PrF 2024 026.

■ REFERENCES

(1) Sharp, J. T. Nitrile Ylides and Nitrile Imines. In *Chemistry of Heterocyclic Compounds 59: Synthetic Applications of 1,3-Dipolar Cycloaddition Chemistry Toward Heterocycles and Natural Products*; Padwa, A., Pearson, W. H., Eds.; John Wiley & Sons: 2002.

(2) Shawali, A. S. Reactions of Heterocyclic Compounds with Nitrilimines and Their Precursors. *Chem. Rev.* **1993**, *93*, 2731−2777.

(3) Herner, A.; Marjanovic, J.; Lewandowski, T. M.; Marin, V.; Patterson, M.; Miesbauer, L.; Ready, D.; Williams, J.; Vasudevan, A.; Lin, Q. 2-Aryl-5-carboxytetrazole as a New Photoaffinity Label for Drug Target Identification. *J. Am. Chem. Soc.* **2016**, *138*, 14609−14615.

(4) Tian, Y.; Jacinto, M. P.; Zeng, Y.; Yu, Z.; Qu, J.; Liu, W. R.; Lin, Q. Genetically Encoded 2-Aryl-5-carboxytetrazoles for Site-Selective Protein Photo-Cross-Linking. *J. Am. Chem. Soc.* **2017**, *139*, 6078−6081.

(5) Zhang, J.; Liu, J.; Li, X.; Ju, Y.; Li, Y.; Zhang, G.; Li, Y. Unexpected Cyclization Product Discovery from the Photoinduced Bioconjugation Chemistry between Tetrazole and Amine. *J. Am. Chem. Soc.* **2024**, *146*, 2122−2131.

(6) Wan, J.; Nytka, M.; Vu, K.; Qian, H.; Lemr, K.; Turecek, F. Nitrile Imines as Peptide and Oligonucleotide Photocrosslinkers in Gas-Phase Ions. *J. Am. Soc. Mass Spectrom.* **2024**, *35*, 344−356.

(7) Vlk, M.; Wan, J.; Nytka, M.; Vu, T. N. K; Lemr, K.; Turecek, F. Photochemical and Collision-Induced Cross-Linking of Asp, Glu, Asn, and Gln Residues in Peptide-Nitrile Imine Conjugate Ions in the Gas Phase. *J. Am. Soc. Mass Spectrom.* **2024**, DOI: 10.1021/jasms.4c00394.

(8) Zhu, H.; Nytka, M.; Vu, T. N. K.; Lemr, K.; Tureček, F. Photochemical and Collision-Induced Cross-Linking in Stereochemically Distinct Scaffolds of Peptides and Nitrile-Imine Conjugate Ions in the Gas-Phase. *J. Am. Soc. Mass Spectrom.* **2024**, *35*, 3070−3088.

(9) Alexander, A. J.; Thibault, P.; Boyd, R. K. Collision-Induced Dissociations of Peptide Ions 2. Remote Charge-Site Fragmentations in a Tandem, Hybrid Mass Spectrometer. *Rapid Commun. Mass Spectrom.* **1989**, *3*, 30−34.

(10) Ballard, K. D.; Gaskell, S. J. Sequential Mass Spectrometry Applied to the Study of the Formation of "Internal" Fragment Ions of Protonated Peptides. *Int. J. Mass Spectrom. Ion Processes* **1991**, *111*, 173−189.

(11) Dongre, A. R.; Jones, J. L.; Somogyi, A.; Wysocki, V. H. Influence of Peptide Composition, Gas-Phase Basicity, and Chemical Modification on Fragmentation Efficiency: Evidence for the Mobile Proton Model. *J. Am. Chem. Soc.* **1996**, *118*, 8365−8374.

(12) Giles, K.; Ujma, J.; Wildgoose, J.; Pringle, S.; Richardson, K.; Langridge, D.; Green, M. A Cyclic Ion Mobility-Mass Spectrometry System. *Anal. Chem.* **2019**, *91*, 8564−8573.

(13) Tureček, F. Covalent Crosslinking in Gas-Phase Biomolecular Ions. An Account and Perspective. *Phys. Chem. Chem. Phys.* **2023**, *25*, 32292−32304.

(14) Řezáč, J.; Fanfrlík, J.; Salahub, D.; Hobza, P. Semiempirical Quantum Chemical PM6Method Augmented by Dispersion and H Bonding Correction Terms Reliably Describes Various Types of Noncovalent Complexes. *J. Chem. Theory Comput.* **2009**, *5*, 1749−1760.

(15) Řezáč, J. Cuby: An Integrative Framework for Computational Chemistry. *J. Comput. Chem.* **2016**, *37*, 1230−1237.

(16) Stewart, J. J. P. *MOPAC 16; Stewart Computational Chemistry*; Colorado Springs, CO, 2016. Accessed October 2024.

(17) Berendsen, H. J. C.; Postma, J. P. M.; van Gunsteren, W. F.; DiNola, A.; Haak, J. R. Molecular Dynamics with Coupling to an External Bath. *J. Chem. Phys.* **1984**, *81*, 3684−3690.

(18) Becke, A. D. Density-Functional Exchange-Energy Approximation with Correct Asymptotic Behavior. *Phys. Rev. A* **1988**, *38*, 3098−3100.

(19) Zhao, Y.; Truhlar, D. G. The M06 Suite of Density Functionals for Main Group Thermochemistry, Thermochemical Kinetics, Noncovalent Interactions, Excited States, and Transition Elements: Two New Functionals and Systematic Testing of Four M06-Class Functionals and 12 Other Functionals. *Theor. Chem. Acc.* **2008**, *120*, 215−241.

(20) Grimme, S.; Ehrlich, S.; Goerigk, L. Effect of the Damping Function in Dispersion Corrected Density Functional Theory. *J. Comput. Chem.* **2011**, *32*, 1456−1465.

(21) Nickerson, C. J.; Bryenton, K. R.; Price, A. J. A.; Johnson, E. R. Comparison of Density-Functional Theory Dispersion Corrections for the DES15K Database. *J. Phys. Chem. A* **2023**, *127*, 8712−8722.

(22) Weigend, F. Accurate Coulomb-Fitting Basis Sets for H to Rn. *Phys. Chem. Chem. Phys.* **2006**, *8*, 1057−1065.

(23) Fishman, V.; Semidalas, E.; Martin, J. M. L. Basis Set Extrapolation from the Vanishing Counterpoise Correction Condition. *J. Phys. Chem. A* **2024**, *128*, 7462−7470.
(24) Singh, U. C.; Kollman, P. A. An Approach to Computing Electrostatic Charges for Molecules. *J. Comput. Chem.* **1984**, *5*, 129−145.
(25) Besler, B. H.; Merz, K. M., Jr.; Kollman, P. Atomic Charges Derived from Semiempirical Methods. *J. Comput. Chem.* **1990**, *11*, 431−439.
(26) Ieritano, C.; Crouse, J.; Campbell, J. L.; Hopkins, W. S. A Parallelized Molecular Collision Cross Section Package with Optimized Accuracy and Efficiency. *Analyst* **2019**, *144*, 1660−1670.
(27) Ieritano, C.; Hopkins, W. S. Assessing Collision Cross Section Calculations Using MobCal-MPI with a Variety of Commonly Used Computational Methods. *Mater. Today Commun.* **2021**, *27*, No. 102226.
(28) Halgren, T. A. Merck Molecular Force Field. I. Basis, Form, Scope, Parametrization, and Performance of MMFF94. *J. Comput. Chem.* **1996**, *17*, 490−519.
(29) Chu, I. K.; Siu, C.-K.; Lau, J. K.-C.; Tang, W. K.; Mu, X.; Lai, C. K.; Guo, X.; Wang, X.; Li, N.; Xia, Y.; Kong, X.; Oh, H. B.; Ryzhov, V.; Turecek, F.; Hopkinson, A. C.; Siu, K.W. M. Proposed Nomenclature for Peptide Ion Fragmentation. *Int. J. Mass Spectrom.* **2015**, *390*, 24−27.
(30) Klassen, J. S.; Kebarle, P. Collision-Induced Dissociation Threshold Energies of Protonated Glycine, Glycinamide, and Some Related Small Peptides and Peptide Amino Amides. *J. Am. Chem. Soc.* **1997**, *119*, 6552−6563.
(31) Paizs, B.; Suhai, S. Fragmentation Pathways of Protonated Peptides. *Mass Spectrom. Rev.* **2005**, *24*, 508−548.
(32) Laskin, J.; Yang, Z.-B.; Song, T.; Lam, C.; Chu, I. K. Effect of the Basic Residue on the Energetics, Dynamics, and Mechanisms of Gas-Phase Fragmentation of Protonated Peptides. *J. Am. Chem. Soc.* **2010**, *132*, 16006−16016.
(33) Mookherjee, A.; Armentrout, P. B. Thermodynamics and Reaction Mechanisms for Decomposition of a Simple Protonated Tripeptide, H^+GGA: From H^+GGG to H^+GAG to H^+GGA. *J. Am. Soc. Mass Spectrom.* **2022**, *33*, 355−368.
(34) Ding, X.; Zhao, S.; Pan, Y. Thermal Hazard and Mechanism Study of 5-(4-Pyridyl)tetrazole (H4-PTZ). *Emerg. Manag. Sci. Technol.* **2022**, *2*, 13.
(35) Yao, H.; Ni, L.; Wu, P.; Jiang, J.; Ni, Y.; Yao, X. Yao, X. Thermal Hazard and Pyrolysis Mechanism of Tetrazolo[1,5-a[puyiridine by TG, DSC, ARC, TG-MS and DTT Methods. *J. Anal. Appl. Pyrol.* **2021**, *159*, No. 105299.
(36) Nguyen, H. T. H.; Andrikopoulos, P. C.; Bím, D.; Rulíšek, L.; Dang, A.; Tureček, F. Radical Reactions Affecting Polar Groups in Threonine Peptide Ions. *J. Phys. Chem. B* **2017**, *121*, 6557−6569.
(37) Liu, Y.; Dang, A.; Urban, J.; Tureček, F. Charge-Tagged DNA Radicals in the Gas Phase Characterized by UV-Vis Photodissociation Action Spectroscopy. *Angew. Chem., Int. Ed. Engl.* **2020**, *59*, 7772−7777.

https://doi.org/10.1021/jasms.4c00438
J. Am. Soc. Mass Spectrom. 2025, 36, 209−220